Self-Assembled Nanometer Lamellae of Thermoelectric PbTe and Sb2Te3 with Epitaxy-like Interfaces

ARTICLE *in* CHEMISTRY OF MATERIALS · NOVEMBER 2006

Impact Factor: 8.35 · DOI: 10.1021/cm062121p

Self-Assembled Nanometer Lamellae of Thermoelectric PbTe and Sb_2Te_3 with Epitaxy-like Interfaces

Teruyuki Ikeda,[†] Lauren A. Collins,[†] Vilupanur A. Ravi,[‡] Franck S. Gascoin,[†] Sossina M. Haile,[†] and G. Jeffrey Snyder*,[†]

Materials Science, California Institute of Technology, 1200 E. Colorado Boulevard, Pasadena, California 91125, and Chemical and Materials Engineering, California State Polytechnic University, 3801 West Temple Avenue, Pomona, California 91768

Received September 7, 2006. Revised Manuscript Received November 17, 2006

Utilizing the decomposition of metastable $Pb_2Sb_6Te_{11}$ into PbTe and Sb_2Te_3, we produced a layered (lamellar) microstructure of PbTe and Sb_2Te_3 in which the interlamellar spacing can be controlled by the temperature and time of the decomposition process. Adjacent PbTe and Sb_2Te_3 lamellae are crystallographically oriented, indicating high-quality epitaxy-like interfaces. Average lamellar spacings as small as 180 nm are observed, corresponding to a PbTe layer thickness of 40 nm. These nanoscale multilayers, formed by bulk processing, resemble thin-film superlattice thermoelectric materials, which have shown exceptionally high thermoelectric efficiency.

The efficiency of a thermoelectric device is governed by the thermoelectric figure of merit, zT, of the component materials, defined as $\alpha^2\sigma T/\kappa$, where α is the Seebeck coefficient, σ the electrical conductivity, and κ the thermal conductivity. Materials investigated and optimized over the past 50 years have largely been conventional, simple semiconductors, with the best of these exhibiting zT values no greater than approximately 1. Examples include alloys of bismuth telluride, lead telluride, and silicon germanium.[1]

Recently, that zT barrier has been broken; $zT > 2$ has been achieved in thin film superlattices or "quantum well" materials with feature sizes of several to tens of nanometers.[2−4] The first significant result has been that of Venkatasubramanian (2001), who demonstrated $zT = 2.4$ using Bi_2Te_3−Sb_2Te_3 quantum well superlattices with 6 nm periodicity. Harman and co-workers prepared quantum dot superlattices in the PbTe−PbSeTe system (described as PbSe nanodots embedded in a PbTe matrix) and demonstrated zT values of 1.6.

Despite the high zT of such thermoelectrics, the performance of devices utilizing superlattice materials has not yet surpassed the performance of bulk Bi_2Te_3-based devices. This is due to the small size of the thermoelectric elements that can be achieved from painstaking "top-down" fabrication methods, which imply a large, relative contribution of electrical and thermal contact resistances. Such losses could be avoided if nanostructured thermoelectric elements could be manufactured on the millimeter as opposed to micrometer scale. Bulk materials with small nanodots have shown promise,[5] but layered structures have not yet been made by bulk methods.

We have chosen rapid solidification and decomposition of thermoelectric composites as a means of obtaining self-assembled nanostructured thermoelectrics in bulk volumes as an alternative to the layer-by-layer top-down methods. Such an approach is justified by the observation that the thermal conductivity reductions responsible for high zT in superlattice structures are predicted even for periodicities of tens to hundreds of nanometers.[6] Furthermore, significant thermal conductivity reduction has been found in both the in-plane[4] and cross-plane[3] directions, indicating that the enhancement in thermoelectric properties occurs regardless of the orientation of the superlattices or nanostructures relative to the measurement direction.[6] Thus, random, self-assembled structures with nanometer to submicrometer feature sizes can be anticipated to result in enhancements to zT, analogous to that observed in superlattice materials.

Rapid solidification of off- and near-eutectic compositions is well-known to yield a variety of microstructures, from dendritic to lamellar in a wide range of pseudobinary systems,[7−9] while providing some control of micrometr scale spacing between the two components. Preliminary studies in the PbTe−Sb_2Te_3 pseudobinary system showed that submicrometer features could not be obtained, even at high cooling rates, because of the formation of a ternary com-

* To whom correspondence should be addressed. E-mail: jsnyder@caltech.edu.
† California Institute of Technology.
‡ California State Polytechnic University.

(1) *CRC Handbook of Thermoelectrics*; Rowe, D. M., Ed.; CRC Press: Boca Raton, FL, 1995.
(2) Caylor, J. C.; Coonley, K.; Stuart, J.; Colpitts, T.; Venkatasubramanian, R. *Appl. Phys. Lett.* **2005**, *87*, 23105.
(3) Venkatasubramanian, R.; Siivola, E.; Colpitts, T.; O'Quinn, B. *Nature* **2001**, *413*, 597−602.
(4) Harman, T. C.; Taylor, P. J.; Walsh, M. P.; LaForge, B. E. *Science* **2003**, *297*, 2229−2232.
(5) Hsu, K. F.; Loo, S.; Guo, F.; Chen, W.; Dyck, J. S.; Uher, C.; Hogan, T.; Polychroniadis, E. K.; Kanatzidis, M. G. *Science* **2004**, *303*, 818−821.
(6) Dames, C.; Chen, G. In *Thermoelectrics Handbook Macro to Nano*; Rowe, D. M., Ed.; CRC Press: Boca Raton, FL, 2006, p 42-1.
(7) Ikeda, T.; Haile, S. M.; Ravi, V. A.; Azizgolshani, H.; Gascoin, F.; Snyder, G. J. *Acta Mater.* **2007**, in press.
(8) Ikeda, T.; Azizgolshani, H.; Haile, S. M.; Snyder, G. J.; Ravi, V. A. In *Proceedings of the 24th International Conference on Thermoelectrics*, Clemson, SC, June 2005; IEEE: New York, 2005; p 132.
(9) Jang, K.-W.; Lee, D.-H. In *Proceedings of the Fourteenth International Conference on Thermoelectrics*, St. Petersburg, Russia, June 1995; IEEE: New York, 1995; p 108.

10.1021/cm062121p CCC: $37.00
Published on Web 01/17/2007

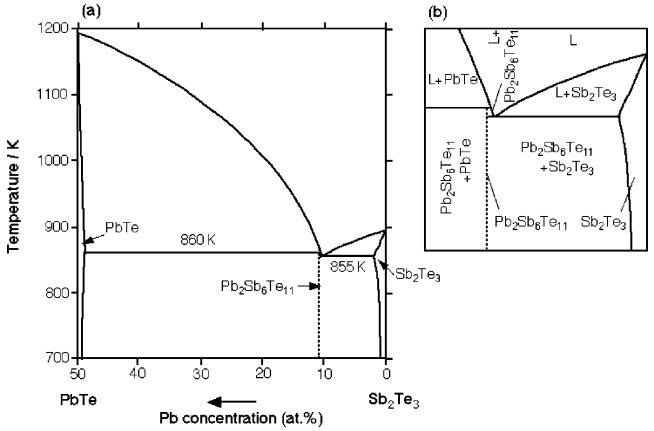

Figure 1. Pseudo-binary phase diagram PbTe−Sb_2Te_3 (after Abrikosov[11]). Here, we show the $Pb_2Sb_6Te_{11}$ phase as a metastable phase. The region near the eutectic reaction is enlarged in (b).

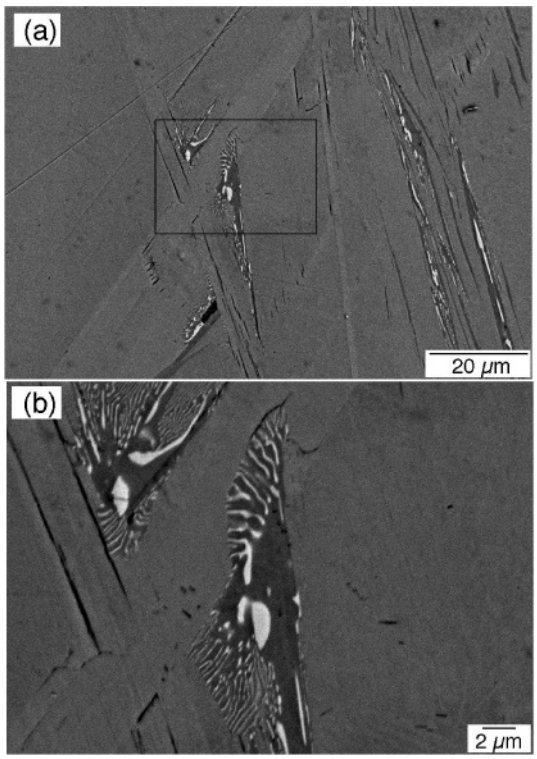

Figure 2. (a) Microstructure of rapidly cooled Pb−Sb−Te eutectic melt. The primary constituent is $Pb_2Sb_6Te_{11}$, and the bright and dark phases are PbTe and Sb_2Te_3, respectively. The rectangular region shown in (a) is enlarged in (b).

pound, $Pb_2Sb_6Te_{11}$, close to the eutectic composition.[7,8] In the present work, we demonstrate that $Pb_2Sb_6Te_{11}$ is metastable and decomposes into submicrometer scale lamellae of PbTe and Sb_2Te_3, where the lamellar spacing can be controlled by adjusting the time and/or temperature of the transformation process.

$Pb_2Sb_6Te_{11}$ was prepared by high-temperature direct synthesis. Lead (Alfa Aesar 99.999%), antimony (Alfa Aesar 99.99%), and tellurium (Alfa Aesar 99.999%) were loaded into 12 mm diameter quartz ampoules in the required stoichiometric ratio and then sealed under a vacuum of approximately 3×10^{-5} Torr to prevent oxidation at high temperatures. Samples were reacted in a high-temperature single-zone vertical furnace for 24 h at 750 °C. Alloys were subsequently water quenched and then annealed at selected

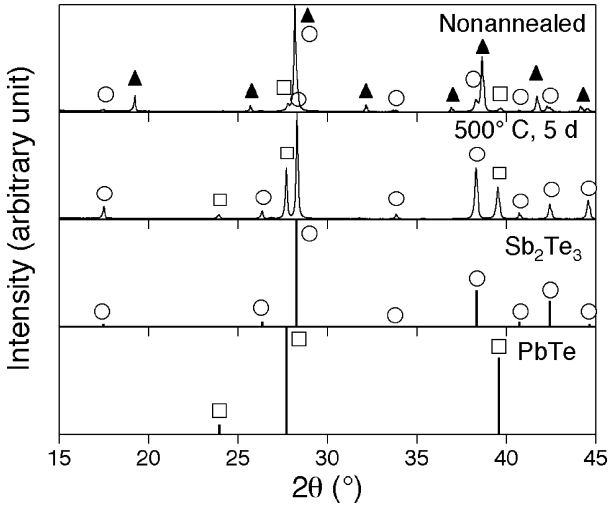

Figure 3. Powder X-ray diffraction before and after annealing (500 °C, 5 days) rapidly cooled $Pb_2Sb_6Te_{11}$. Open circles show the peaks of Sb_2Te_3 (○) and squares those of PbTe (□). Peaks shown by triangles are those of $Pb_2Sb_6Te_{11}$ (▲) phase.

temperatures from 200 to 500 °C for periods of 15 min to 5 days.

The resulting ingots were cut, mounted in epoxy pucks, and polished finally with 0.3 μm Al_2O_3 paste. The microstructures were observed using a field emission scanning electron microscope (Carl Zeiss LEO 1550 VP) equipped with a Robinson backscattered electron (BSE) detector for its high compositional contrast capabilities. The accelerating voltage was 20 kV. The chemical compositions of the constituent phases in each alloy were measured using an energy-dispersive X-ray spectrometer (EDS, INCAEnergy energy dispersion X-ray microanalysis system, Oxford Instruments) or a wavelength-dispersive X-ray spectrometer (WDS, JXA-8200, JEOL Ltd.). For the WDS measurements, Sb, Te, and PbS samples were used as standards for ZAF conversion from intensities of Pb M_α, Sb L_α, and Te L_α to concentrations. The crystallographic orientations in the microstructures were determined using the electron backscatter diffraction technique (EBSD; HKL Technology, Inc.). For these measurements, the surface of samples were finally polished with colloidal silica (50 nm). The operating voltage of the electron microprobe was 20 kV. The surface of the samples was inclined at 70° to the vertical direction with respect to the electron beam. Electron backscatter patterns over areas of 11.2×5 μm^2 were mapped in steps of 0.2×0.2 μm^2 and analyzed using the commercial software package Channel 5 (HKL Technology, Inc.).

Features of the microstructure, including lamellar spacing, and volume fractions of the resulting phases were quantified using image analysis software (Mac Scope, Mitani Corp.) To determine the distribution of lamellar spacing, we measured the distances between all neighboring lamellae in at least seven SEM images (one image typically includes 200−600 lamellae).

X-ray diffraction (XRD) (Phillips X-Pert Pro diffractometer, Cu K-α radiation, $20° \leq 2\theta \leq 70°$) was performed on powder samples to identify phases and their crystal structure.

The pseudobinary system examined here is comprised of two largely immiscible compounds: PbTe−Sb_2Te_3, where

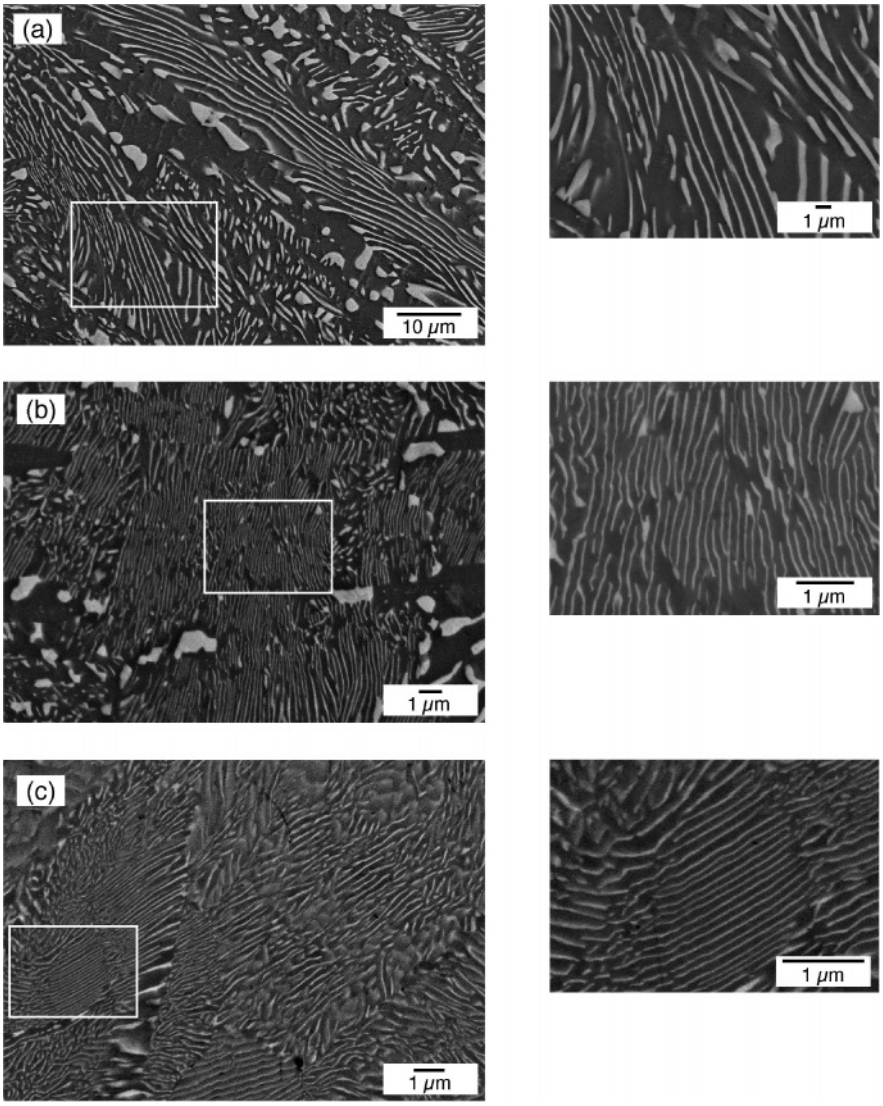

Figure 4. Microstructure of $Pb_2Sb_6Te_{11}$ transformed into Sb_2Te_3- and PbTe-rich regions by annealing. The lighter regions are PbTe, the darker regions Sb_2Te_3. The different layer spacings in the larger figure are due to orientation differences of individual grains. (a) Annealing at 500 °C for 5 days; (b) annealing at 400 °C for 5 days; (c) annealing at 300 °C for 5 days.

both end members individually exhibit good thermoelectric properties.[10] The phase $Pb_2Sb_6Te_{11}$ has a crystal structure distinct from that of PbTe and Sb_2Te_3 but is not found in some of the phase diagrams because it is metastable, as demonstrated below. The proposed nonequilibrium phase diagram is shown in Figure 1. Two invariant reactions are of relevance, i.e., a peritectic reaction, L + PbTe = $Pb_2Sb_6Te_{11}$ and a eutectic reaction, L = $Pb_2Sb_6Te_{11}$ + Sb_2Te_3.

Even without significant effort to cool rapidly, the mixed-crystalline phase $Pb_2Sb_6Te_{11}$ forms. Compositional analysis using EDS indicated that the majority phase has composition $Pb_{9.66}Sb_{32.64}Te_{57.69}$ (identified as "$Pb_2Sb_6Te_{11}$" in ref 11) very near the reported eutectic composition $Pb_{9.84}Sb_{32.12}Te_{58.03}$.[11] The $Pb_2Sb_6Te_{11}$ phase is >98 vol % of the sample. The remaining <2 vol % is composed of PbTe (containing 6 at % Sb), visible as a bright phase in electron backscatter images and a darker phase that is Sb_2Te_3 (containing 2−3 at % Pb) (Figure 2). These compositions were also observed from eutectic solidification.[7,8] The PbTe phases in this composition can have a range of microstructural morphologies ranging from globular to dendritic, with limited regions of the fine microstructure that will be described in more detail below. Powder X-ray diffraction patterns (Figure 3) obtained from water quenched samples (containing 99% $Pb_2Sb_6Te_{11}$) show that the structure of this compound is essentially that of $PbSb_2Te_4$, reported by Shelimova et al.[12] ($R\bar{3}m$, a = 0.4350 nm and c = 4.1712 nm).

Upon annealing, the $Pb_2Sb_6Te_{11}$ phase decomposes into submicrometer scale layers of PbTe and Sb_2Te_3 (Figure 4). A 5 day anneal at 500 °C completely decomposes $Pb_2Sb_6Te_{11}$ into a lamellar structure (Figure 4a). These decomposition products are well-crystallized with the expected PbTe and Sb_2Te_3 structures, as confirmed by XRD (Figure 3).

The lamellae in Figure 4 occur in regions, loosely termed grains (with grain size on the order of 10−30 μm), within which the lamellae are all in the same direction and uniformly

(10) Wood, C. *Rep. Prog. Phys.* **1988**, *51*, 459−539.
(11) Abrikosov, N. K.; Elagina, E. I.; Popova, M. A. *Inorg. Mater.* **1965**, *1*, 1944.
(12) Shelimova, L. E.; Karpinskii, O. G.; Svechnikova, T. E.; Avilov, E. S.; Kretova, M. A.; Zemskov, V. S. *Inorg. Mater.* **2004**, *40*, 1264−1270.

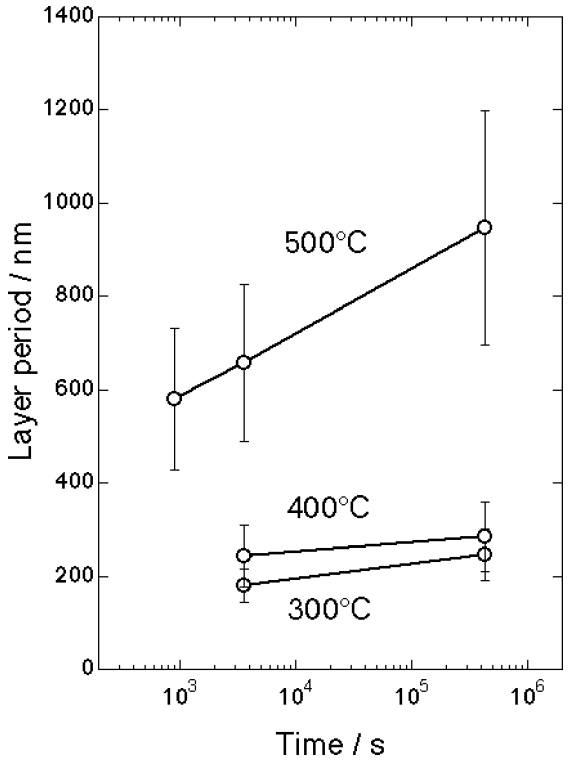

Figure 5. Average layer period of Sb_2Te_3 and PbTe decomposed regions showing the decrease in lamellae spacing as the temperature or time of annealing is reduced. Error bars show the standard deviation of lamellar spacing distribution.

spaced. The lamellar spacing for different grains appears to vary considerably. The apparent variation in lamellar spacing from grain to grain is largely due to differences in orientation of individual grains. Lamellae that happen to be perpendicular to the specimen surface have the smallest spacing, whereas those that are nearly coplanar to the specimen surface appear to have much larger spacing. Thus, not only is the interlamellar spacing narrower than that suggested by the images, the true interlamellar spacing is closest to that seen in the grains with the finest microstructure. Assuming a random orientation of grains, we modeled the average layer spacing (defined as the full wavelength of compositional variation) and the distribution width following ref 13; these are the quantities discussed hereafter.

The spacings between the lamellae noticeably increased with both the temperature and time of annealing (whereas the amount of remaining $Pb_2Sb_6Te_{11}$ decreased), Figure 5. Accordingly, the finest interlamellar spacing of 179 nm was observed after a 3 h anneal at 300 °C. This spacing implies, on the basis of the overall alloy composition and by image analysis, Sb_2Te_3 layers that are 140 nm thick and PbTe layers 39 nm thick. These layers are 100−1000 times thicker than those of the complex layered structures observed by X-ray diffraction in the similar PbTe−Bi_2Te[12] and PbSe−Bi_2Se[14] systems. In the latter system, in particular, the principle of phase homologies[14] has been exploited to generate structures in which the crystallographic unit cell is composed of atomic layers that are structurally similar to those in the end-member phases. Unlike in the phase homology compounds, in the lamellae shown here, no fully coherent unit cell may be drawn containing an entire lamellar structure, as the layer thickness and direction are not sufficiently periodic.

Metallurgical systems in which similar solid−solid transformations ($S \rightarrow \alpha + \beta$) occur and lead to highly regular structures have been studied in depth and can serve as a basis for understanding the observations made here. For example, the well-known Guinier−Preston (GP) zones occurring in aluminum alloys are nanosized, coherent, and metastable particles produced en route to the eventual incoherent equilibrium end product, e.g., $CuAl_2$ in Al−4 wt % Cu (for recent discussions, see refs 15 and 16). Other solid−solid reactions, in particular eutectoid reactions, such as the well-known austenite to pearlite transformation in steels, often form lamellae similar to the ones seen in Figure 4, as do lamellar eutectic structures.[17]

For a eutectoid decomposition process, the layer spacing λ is expected to change with time t and absolute temperature T according to $\lambda - \lambda_0 = KDt/T$, where D is the diffusion coefficient and K is a geometric factor.[17] Following Hillert,[18] the layer spacing at the initiation of growth, λ_0, is $\lambda_0 = 4\gamma T_E V_m/\Delta H \Delta T$, as derived from the minimum thermodynamic size at nucleation. Here, γ is the surface energy, T_E is the eutectoid invariant temperature, ΔT and ΔH are the temperature and enthalpy difference of the supercooled material at the point of nucleation compared to T_E, and V_m is the molar volume. The increase in interlamellar spacing with time evident in Figure 5 is clearly expected from these relationships, although the linear dependence with time cannot be verified.[19] Its increase with temperature suggests that λ_0 strongly depends on temperature, most likely via its dependence on ΔT.

From an examination of partially decomposed regions, Figure 7, it appears that the lamellae grow into the undecomposed $Pb_2Sb_6Te_{11}$ in a typical eutectoid manner such that the lamellae are preferentially oriented perpendicular to the interface between the undecomposed and decomposed regions. The grain boundaries of the undecomposed $Pb_2Sb_6Te_{11}$, which may contain a thin layer Sb_2Te_3 as a grain boundary phase,[7] appear to nucleate as well as stop the growth of the lamellae.

The PbTe−$Pb_2Sb_6Te_{11}$−Sb_2Te_3 system displays rather remarkable features in the crystallographic orientation between component phases, as determined by the EBSD analyses. Within the decomposed regions, pole figures (Figure 6) show that adjacent Sb_2Te_3 and PbTe lamellae are oriented such that the <001> basal planes of Sb_2Te_3 are parallel to one of the <111> planes of PbTe. These correspond to the close-packed Te planes in the respective structures, and the lattice mismatch is only about 6%.

(13) Pellissier, G. E.; Hawekes, M. F.; Johnson, W. A.; Mehl, R. F. *Trans. ASM* **1942**, *30*, 1049.
(14) Kanatzidis, M. G. *Acc. Chem. Res.* **2005**, *38*, 359−368.
(15) Gottstein, G. *Physical Foundations of Materials Science*; Springer: New York, 2004.
(16) Reed-Hill, R. E.; Abbaschian, R. *Physical Metallurgy Principles*; PWS Publishing Company: Boston, 1994.
(17) Graham, L. D.; Kraft, R. W. *Trans. Metall. Soc. AIME* **1966**, *236*, 94.
(18) Hillert, M.; Averbach, B. L.; Cohen, M. *Acta Metall.* **1956**, *4*, 31−36.
(19) Ikeda, T.; Ravi, V. A.; Collins, L. A.; Haile, S. M.; Snyder, G. J. In *Proceedings of the 25th International Conference on Thermoelectrics*, Vienna, Austria, Aug 6−10, 2006; IEEE: New York, 2006; in press.

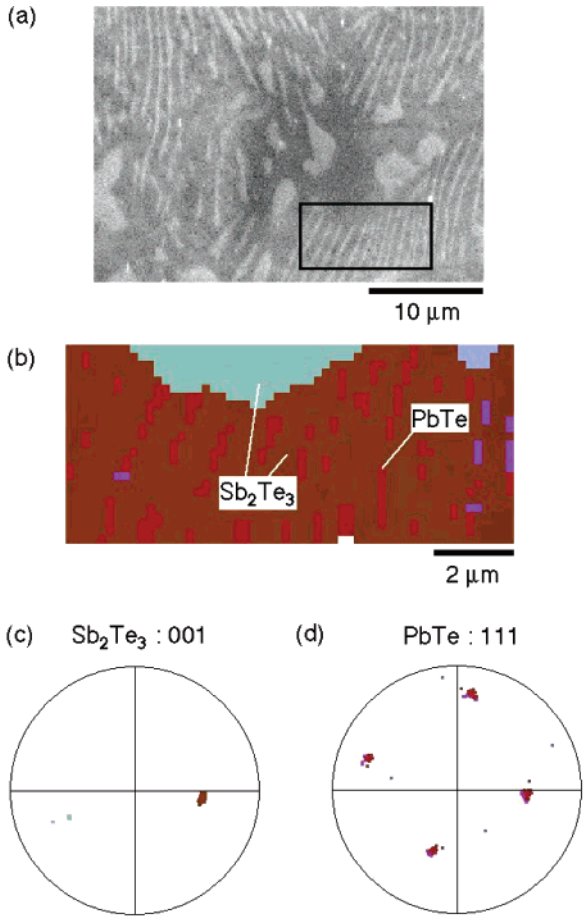

Figure 6. EBSD analysis showing adjacent PbTe and Sb_2Te_3 lamellae have epitaxy-like orientation on a sample annealed at 500 °C for 5 days. (a) Scanning electron image. (b) EBSD mapping obtained from the region shown in (a). (c) Pole figures of the basal planes of Sb_2Te_3. (d) Pole figure of {111} planes of PbTe. Each point in the mappings corresponds to the point that has the same color in the pole figures.

Surprisingly, the lamellae planes (the interface between the lamellar Sb_2Te_3 and PbTe phases) have little preferred crystallographic orientation. Thus the growth of the lamellae can occur in different crystallographic orientations. Moreover, there is no obvious correlation between the crystallographic orientation of undecomposed $Pb_2Sb_6Te_{11}$ and that of the product phases.

Overall, these features raise the possibility that the lamellar growth direction and hence orientation can be controlled via further control of the crystallization conditions by employing, for example, a temperature gradient or heterogeneous nucleation sites.

That the decomposition phases Sb_2Te_3 and PbTe are highly oriented with respect to one another, a characteristic typical of epitaxial crystal growth, suggests the presence of clean, atomically precise interfaces. The presence of such interfaces within nanoscale superlattices may be critical to the high performance of nanostructured thermoelectrics. Both the extraordinary results of Venkatasubramanian and Harman are based on epitaxially grown materials. Poor interfaces between layers is likely to add to the scattering of electrons and result in an increase in electrical resistivity. High electrical resistivity due to interface resistance is the primary challenge for using solution grown nanoparticles, such as PbSe,[20] for thermoelectric applications.

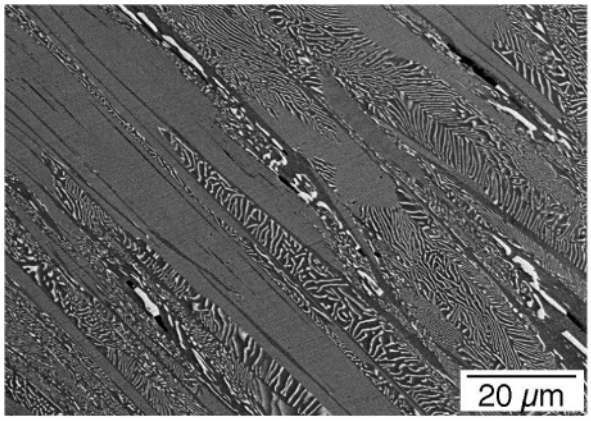

Figure 7. Partially decomposed region (500 °C, 15 min) showing that the lamellae grow along the layer direction with their ends preferentially at the interface between the transformed and untransformed regions.

For utilization in thermoelectric devices, the charge-carrier concentration of this material must be further optimized. The samples described above are p-type with high carrier concentration (Seebeck 30 μV/K and electrical resistivity 4 $\times$ 10^{-4} Ω cm). The high carrier concentration will further make the thermal conductivity large because of the electronic contribution to thermal conductivity from the Wiedemann−Franz law. Thus, to properly evaluate the thermoelectric performance, including thermal conductivity, we will need to reduce the p-type carrier concentration through chemical doping. Preliminary investigations show that at least some reduction in carrier concentration is possible.

Acknowledgment. We thank the Office of Naval Research (Grant N000140610364), the National Science Foundation through Caltech's Center for the Science and Engineering of Materials (CSEM), and the JPLUS program (LC) for their funding of this work.

CM062121P

(20) Sashchiuk, A.; Amirav, L.; Bashouti, M.; Krueger, M.; Sivan, U.; Lifshitz, E. *Nano Lett.* **2004**, *4*, 159−165.